

A measurement of absolute efficiency of the ARAPUCA photon detector in Liquid Argon

Dante Totani^a, Gustavo Cancelo^b, Flavio Cavanna^b, Carlos O. Escobar^b, Ernesto Kemp^c, Franciole Marinho^d, Laura Paulucci^e, Dung D. Phan^f, Stuart Mufson^g, Chris Macias^g, and David Warner^h

^aUniversità degli Studi dell'Aquila, L'Aquila, 67100, Italia

^bFermi National Accelerator Laboratory, Batavia, IL 60510, USA

^cUniversidade Estadual de Campinas, Campinas - SP, 13083-970, Brazil

^dUniversidade Federal de São Carlos, Araras - SP, 13604-900, Brazil

^eUniversidade Federal do ABC, Santo André - SP, 09210-580, Brazil

^fUniversity of Texas at Austin, Austin, TX 78712, USA

^gIndiana University, Bloomington, IN 47405, USA

^hColorado State University, Fort Collins, CO 80523, USA

August 13, 2020

Abstract

In the Fall of 2017, two photon detector designs for the Deep Underground Neutrino Experiment (DUNE) Far Detector were installed and tested in the TallBo liquid argon (LAr) cryostat at the Proton Assembly (PAB) facility, Fermilab. The designs include two light bars developed at Indiana University and a photon detector based on the ARAPUCA light trap engineered by Colorado State University and Fermilab. The performance of these devices is determined by analyzing 8 weeks of cosmic ray data. The current paper focuses solely on the ARAPUCA device as the performance of the light bars will be reported separately. The paper briefly describes the ARAPUCA concept, the TallBo setup, and focuses on data analysis and results.

1 Introduction

The efficiency of photon detectors is of paramount importance for large volume LAr experiments. The detection of scintillation light generated as charged particles traverse a large liquid argon time-projection chamber (LArTPC) adds valuable information to the study of weakly-interacting particles. Most importantly, the leading edge of the scintillation light pulse yields sub-mm precision in reconstructing the absolute position of the event in the drift direction [1]. In addition, the scintillation light can provide the trigger for baryon number violation events, such as proton decay and neutron-antineutron oscillations, and supernova neutrinos, as well as improve rejection of uncorrelated cosmic backgrounds. Given the enormous volume of future experiments such as DUNE (Deep Underground Neutrino Experiment) [2], the photon detectors must cover a large surface area in a cost-effective manner. Several technologies and implementations have been proposed and tested. A relatively novel technology is based on a light trapper device designed by A. Machado and E. Segretto named ARAPUCA [3]. ARAPUCAs are able to increase the effective photon collection area while keeping the sensor area small. The latter property allows a relatively high photon collection efficiency at a reasonable cost. The following paper reports on the

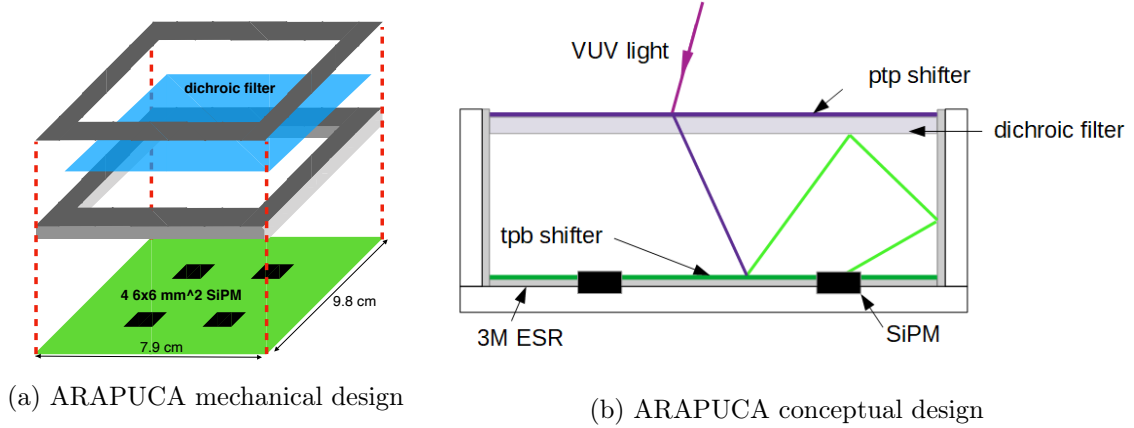


Figure 1: ARAPUCA light trapper device.

design and evaluation of a photon detector unit composed of eight ARAPUCA cells. The detector was placed along a photon detector plane that also included two wavelength shifting light guides from the photon detector group at Indiana University [4]. The combined photon detector set operated for eight weeks in the TallBo LAr cryostat at the PAB facility, Fermilab.

1.1 The ARAPUCA Light Trap

The 128 nm scintillation light from interactions of charged particles in LAr is not detectable directly by affordable sensors such as the traditional photomultipliers (PMTs) or the newer silicon photomultipliers (SIPMs) without appropriate wavelength shifter coating. Among available photon detectors, SIPMs are gaining popularity due to its superior quantum efficiency (QE), desired physical and electrical properties as well as a low cost of production. However, due to their small size, their effective light collection area per unit is easily surpassed by PMTs. The ARAPUCA concept [3] brings up a solution to this problem. As shown in Figure 1b the ARAPUCA consists of two wavelength shifters, a dichroic filter, a highly reflective box and photosensors (SIPMs). The face of the box is used to augment the photon collection area. The VUV photons that enter the light collecting surface of an ARAPUCA device are wavelength-shifted by 200 $\mu\text{g}/\text{cm}^2$ of p-terphenyl deposited on the external face of a dichroic filter. The dichroic filter allows the converted photons to go through and

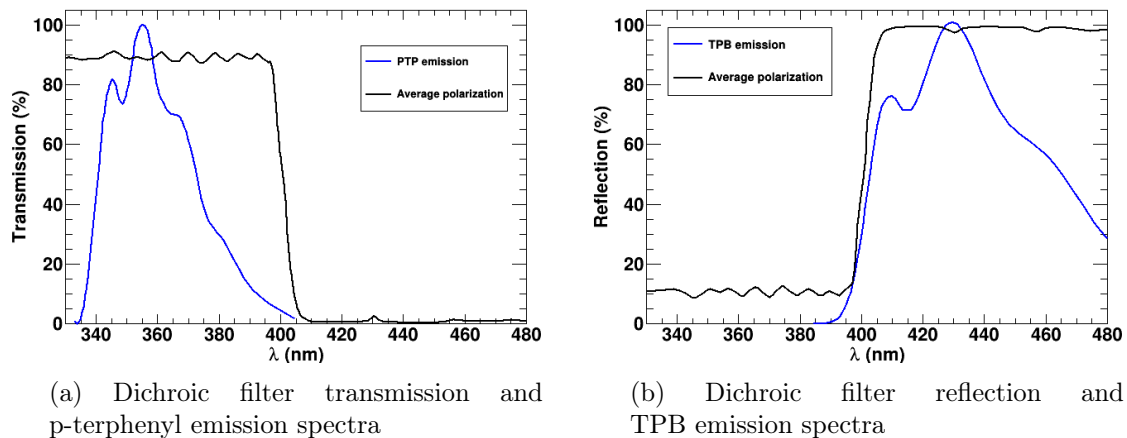


Figure 2: Double coated dichroic filter and wavelength shifter spectra

enter the box. Those photons are wavelength shifted a second time using $250 \mu\text{g}/\text{cm}^2$ of tetra-phenyl butadiene (TPB) deposited on the internal face of the dichroic filter. Since the wavelength cutoff of the dichroic filter is in between the emission spectrum of p-terphenyl and the emission spectrum of TPB, the twice shifted photons remain trapped inside the reflective box and bounce off the walls until they hit the sensors. Figure 1a shows one of the mechanical designs of the ARAPUCA. Several iterations of ARAPUCAs have been studied with variable box sizes, number of SIPMs and location of the SIPMs. In one of the experiments with previous versions of the ARAPUCAs, also performed at TallBo during the Spring 2017 with a radioactive source to excite the LAr, we measured an efficiency $\sim 0.4\%$ [5], considerably lower than the values reported with the new configuration used in this work (see section 3.6.2). The Fall 2017 TallBo experiment used 8 ARAPUCA units of $9.8 \text{ cm} \times 7.9 \text{ cm}$ with 4 SensL $6 \text{ mm} \times 6 \text{ mm}$ SIPM biased at 25.5 V . Figure 2a and 2b show that the emission spectra of p-terphenyl and TPB do not overlap; and the wavelength cutoff of the dichroic filter is located between the two spectra. The peak of the p-terphenyl spectrum is 360 nm , the peak of the TPB spectrum is 430 nm , and the cutoff of the filter is 400 nm .

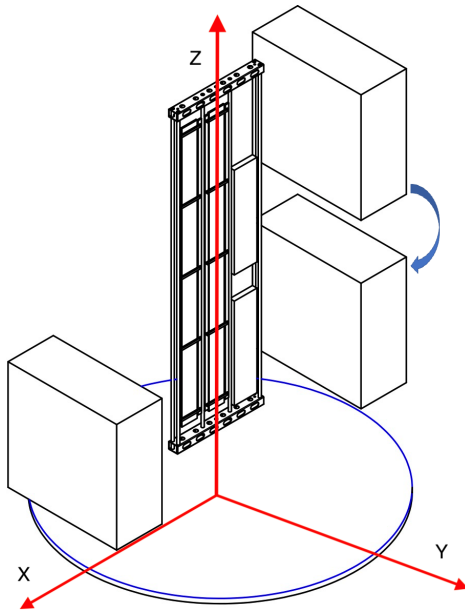


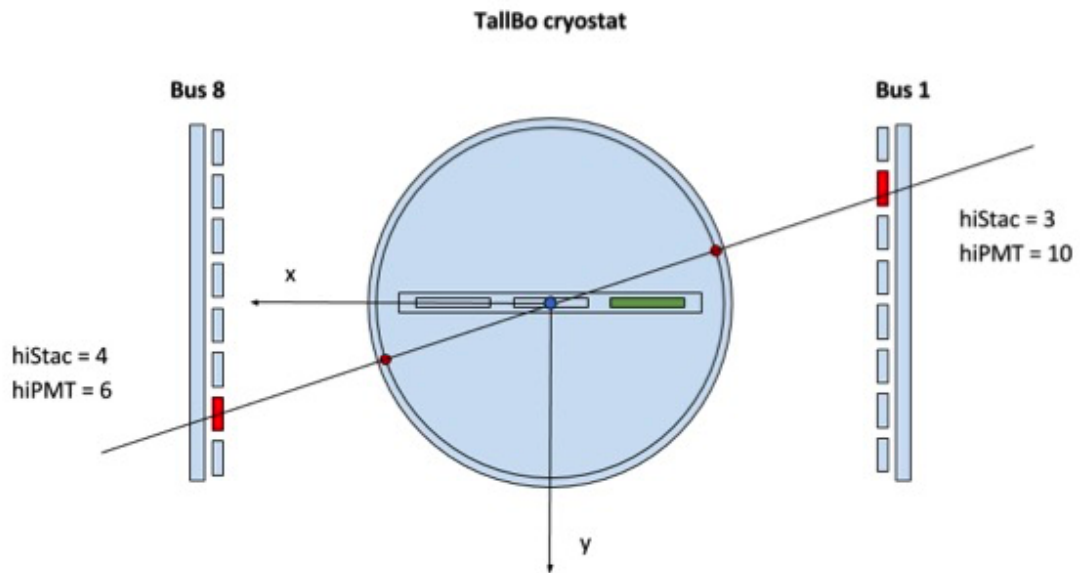
Figure 3: 3D view of the TallBo LAr cryostat.

2 Experimental Setup

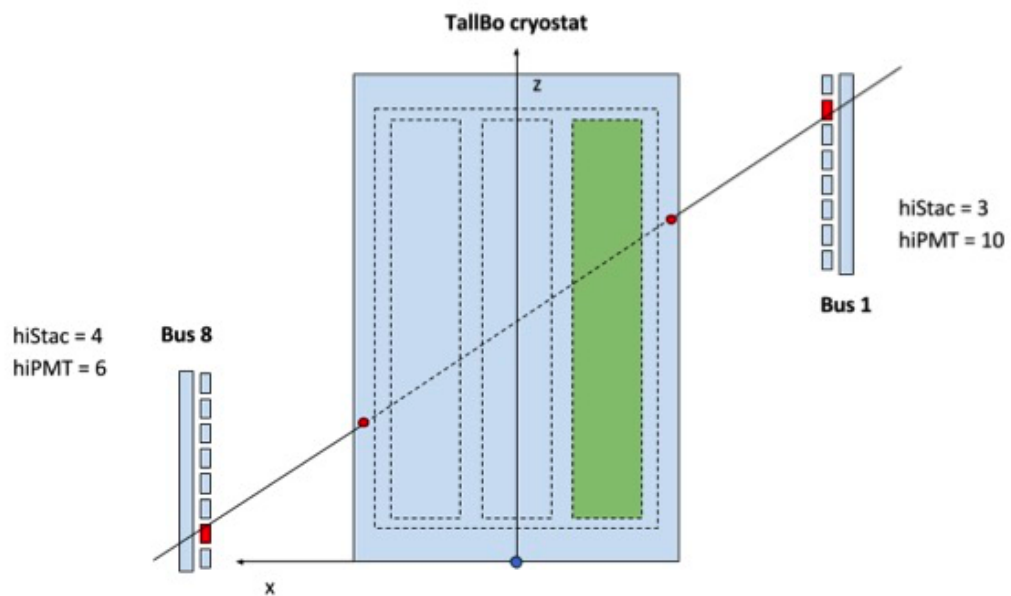
2.1 The TallBo cryostat and hodoscope

The vessel's external diameter is 61.82 cm and the inner diameter is 55.88 cm . The full capacity of TallBo is 460 l . For this experiment TallBo was filled with approximately 350 l of liquid argon. The total thickness of stainless steel presented to a cosmic ray particle that crosses the cryostat is 5.08 cm . The liquid Argon purity in TallBo was monitored using commercial gas analyzers. During the period of the data acquisition the levels of N_2 , H_2O , and O_2 were well below 1 ppm ($\text{ppm} = \text{part per million}$). Typical values were: $N_2 \sim 230 \text{ ppb}$, $H_2O \sim 2 - 3 \text{ ppb}$ and $O_2 \sim 30 \text{ ppb}$ ($\text{ppb} = \text{part per billion}$).

The experiment's trigger used a set of two scintillation paddles and a tracking mechanism based on scintillation paddles and hodoscopes. The hodoscopes were used before in the CREST balloon flight experiment [6, 7]. The hodoscope modules were installed on opposite sides of the TallBo cryostat to select single-track cosmic-ray muons passing through the



(a) Top view.



(b) Front view.

Figure 4: Cross-sectional views of the TallBo LAr cryostat.

2.3 Data Acquisition System

Signals are processed by the SiPM Signal Processor (SSP) module designed by the Electronics Group of the High Energy Physics division at Argonne National Laboratory [8]. The SSP is a 14 bit, 150 MS/s, 12-channel waveform digitizer DAQ. The ADC has a full-scale dynamic range of 2 V and a preamplifier gain of 18.8 V/V. For typical SiPM gains and ganging configurations the SSP allows large signals equivalent ~ 1000 PEs before the ADC saturates. The SSP input noise is $\sim 16 \mu\text{V}$. Each acquired waveform contains 1950 ADC values sampled at 150 MS/s, aggregating to an acquisition time of 13 μs . Each sample bin, 6.67 ns long, is called *tick*. The SSP can trigger internally on each individual channel or externally via external trigger input. The self-trigger mode was used to take calibration data while the external trigger mode with the hodoscope as the trigger source was employed for the cosmic ray run.

2.4 Trigger issues

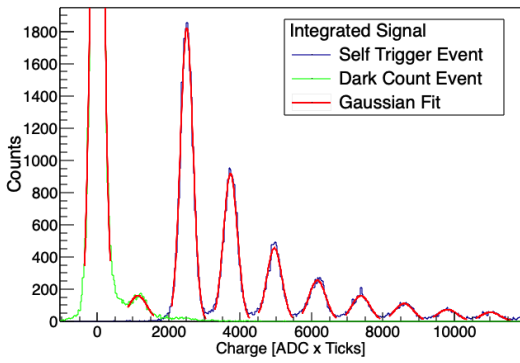
The hodoscope trigger malfunctioned during the experiment. A mistake in the way the coincidence logic was set up caused the trigger to fire more often than expected. The logic performed an OR instead of an AND in two of the channels. Therefore, the trigger not only fired on valid tracks but also on coincidental PMT dark counts of the hodoscope arrays located at the left and right of the dewar during the defined trigger window (150 ns). The collected data set contained a large amount of unusable data that did not represent valid tracks. As shown in the next sections, most of the events were triggered by coincidence of PMT dark counts and contained no signals from the photon detectors, neither in the ARAPUCAs nor the IU light guides. Other spurious events contained partial tracks that did not generate a trigger but were captured by chance during a dark count coincidence event. The hodoscope trigger problem made the analysis of the data challenging, since offline filters had to be devised and applied to the data. However, it also showed the potential of the ARAPUCA architecture given that those filters could have not been applied without the segmentation property of the ARAPUCAs, as will become clear in the next sections of the paper.

3 Data analysis

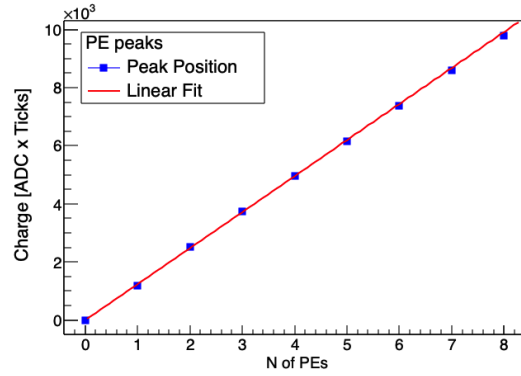
3.1 Calibration

During calibration runs the ARAPUCA signals were acquired by the SSP single channel self trigger mode, using an amplitude threshold slightly above 1 PE. Since the threshold was higher than the single photon electron the histogram is able to exhibit the 2nd peak and higher (Figure 6a blue histogram). The first PE was recovered looking at dark counts in a different integration window (Figure 6a green histogram), far from the trigger point. The first integration window, containing the self trigger point, was in the first half of the waveform (from 100 to 900 *ticks*) and the second window, containing possible dark counts, in the second half of the waveform (from 900 to 1700 *ticks*). Figure 6b shows the linearity of the calibration. The linear fit in Figure 6b is obtained using the means of the Gaussian distribution peaks of Figure 6a. The integrated charge value ($ADC \cdot Ticks$) due to one PE can be obtained by the slope of the straight line.

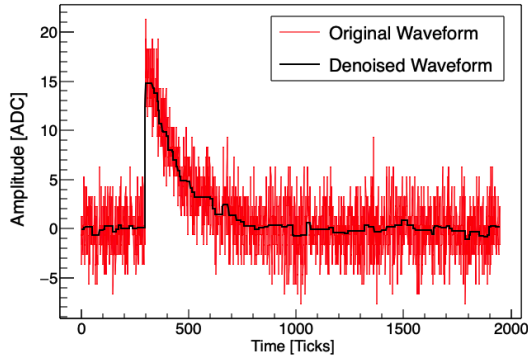
A second procedure was developed to cross check values using the calibration constants obtained from the calibration run. A smaller set of data triggered with the hodoscope was used. Baseline and noise levels were obtained as the mean and root mean square (RMS) for the first 100 points of the signal amplitude for each channel per event. After baseline subtraction a filtering algorithm was used that suppresses random noise but keeps the main



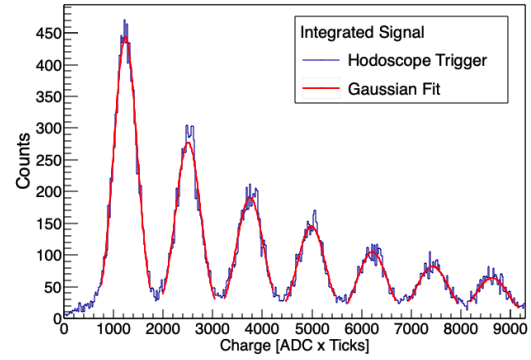
(a) Self triggered and dark count data spectra. In red is shown the multi gaussian fit.



(b) Linear fit for the peak positions. Statistical error bars are smaller than symbols.



(c) Original and denoised waveform comparison.



(d) Hodoscope triggered data spectrum and multi gaussian fit.

Figure 6: Calibration procedures for ARAPUCA 1. The slope of linear fit (b) gives the calibration in $(ADC \cdot Ticks)/PE$.

features of the signal, in particular the fast transitions [9]. A peak finding algorithm was then devised to find peaks and integrate the charge under a peak. Figure 6c shows an example of a peak found. The red line shows the raw data and the black line indicates the filtered signal. The threshold for detecting a pulse has been set to 3σ of the baseline noise (e.g. 8.2 ADC). Figure 6d shows the spectrum obtained with peaks from ARAPUCA 1 (the same used to show the self trigger events analysis). Notice that the pedestal is almost suppressed by the denoising procedure and threshold requirement. A multi Gaussian fit was performed to obtain the charge value for each peak. A linear fit of the peaks as a function of the photon electron number provided the average calibration constants which are in agreement with the self trigger events analysis.

3.2 Data analysis: background rejection

As mentioned in subsection 2.4 most of the data recorded by the experiment was due to the background, since the majority of the triggers were generated by coincidental dark counts in the hodoscope PMTs. Nevertheless, the system has also properly triggered on real tracks (i.e. MIPs), although these events only constituted a small fraction of the stored data, of the order of 5% to 10%.

Since the dark counts are uncorrelated with light in the cryostat most events of that type

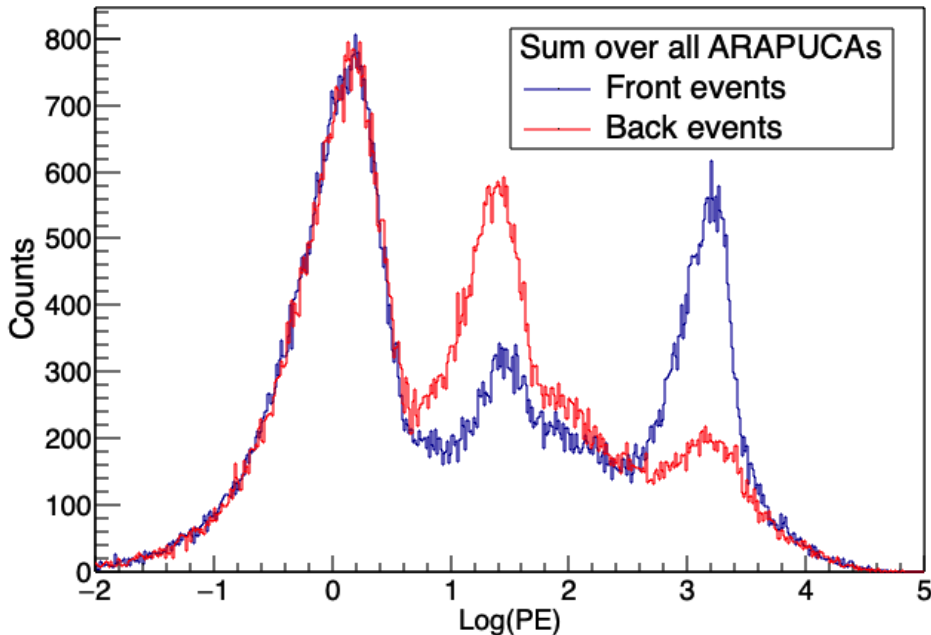


Figure 7: Log(PE) spectra for events triggered as "front" (blue) and "back" (red). The same number of events for both spectra are used, this normalization is reflected in having the same amount of empty events (first peak in both spectra). The excess of events in the second peak of the red spectrum respect the blue one is interpreted as back tracks associated to the right trigger information. In the same way the excess of events in the third peak of the blue spectrum respect the red one is interpreted as front tracks associated to the right trigger information. All common parts of the spectra are interpreted as background: empty events (first peak) and spurious hodoscope coincidences.

were empty or captured incidental background light. Most of these events collected few PEs from radiogenics or very low light background in the TallBo cryostat. A fraction of those events also captured an incidental track that fell within the 150 ns trigger window. Most of those tracks are partial tracks that only passed through one hodoscope arm or none at all. In either case the track position information given by the hodoscope is incorrect, since it corresponds to the hot PMTs which generated the trigger and not to the passage of the track.

The tested version of ARAPUCAs were single sided detectors having filters on only one side. Therefore only tracks passing in front of the ARAPUCA plane could be seen. In this particular occasion, due to the high trigger rate, the comparison between the spectra of events passing in front of the single sided ARAPUCAs and behind them was useful to do event discrimination. It was possible to get information comparing the spectra of events triggered as tracks located entirely in front of the plane containing the windows and behind it. That allowed tracks uncorrelated with trigger position information to be filtered out.

As a first step we considered the spectrum of the number of PEs seen by all ARAPUCAs in the detector, for a given event (PE_{tot}). We obtained individual spectra for two groups of events. Group 1 (blue spectrum of Figures 7) has all events for which the trigger geometry given by the hodoscope labeled a track as passing in front of the ARAPUCA window plane (front events) and Group 2 (red spectrum of Figures 7) with all events passing behind the ARAPUCA window plane (back events). Events that have an entry point in the front and the other one in the back or vice-versa were discarded, like the example in Figures 4a. The

difference between the back and front spectra is the only feature which can be associated to the information coming from the hodoscopes. To enhance the peak display in the spectra, instead to use the PE number, it has been chosen to show the common logarithm of the PE number in plots.

The spectra, reported in Figures 7, show three peaks:

- the first, the largest one, is composed of events for which two crystals fired but negligible light is seen by any ARAPUCA, indicating these are completely random triggers, due to the high hodoscope rates. The fact that both back and front spectra show the first peak identically confirms its origin. The same number of events for both spectra are used.
- the excess of events in the second peak of the red spectrum respect the blue one is interpreted as back tracks associated with a MIP triggering the crystals for a track located entirely behind the ARAPUCAs plan (back track).
- in an equivalent way, the excess of events in the third peak of the blue spectrum respect the red one is interpreted as front tracks associated with a MIP triggering the crystals for a track located entirely in front of the ARAPUCAs plan (front track).

All common parts of the spectra are interpreted as background: empty events (first peak) and spurious hodoscope coincidences.

Similar considerations can be made for each single ARAPUCA. Applying cuts on the minimum and maximum number of PEs collected by each ARAPUCA, it is possible to get a selected dataset of events. Single ARAPUCA cuts, shown as black lines in 9, consist in removing events for which the back spectrum (red in 9) has more events respect to the front spectrum (blue in 9). The front and back spectra show a different behavior for each of the eight ARAPUCAs. The reason of that is the geometrical effect due to the position of the ARAPUCA cells respect the tracks selected by the hodoscope. For this reason the cut needed is different for each ARAPUCA, black lines in Figure 9.

Looking at the sum of the detected PE over the 8 ARAPUCA for the selected events, red spectrum in Figure 8b, they are compatible with the excess of events in the third peak of the blue spectrum in Figure 7. Events remained, black spectrum in Figure 8a, are compatible with the common parts of the spectra in Figure 8b, interpreted as background.

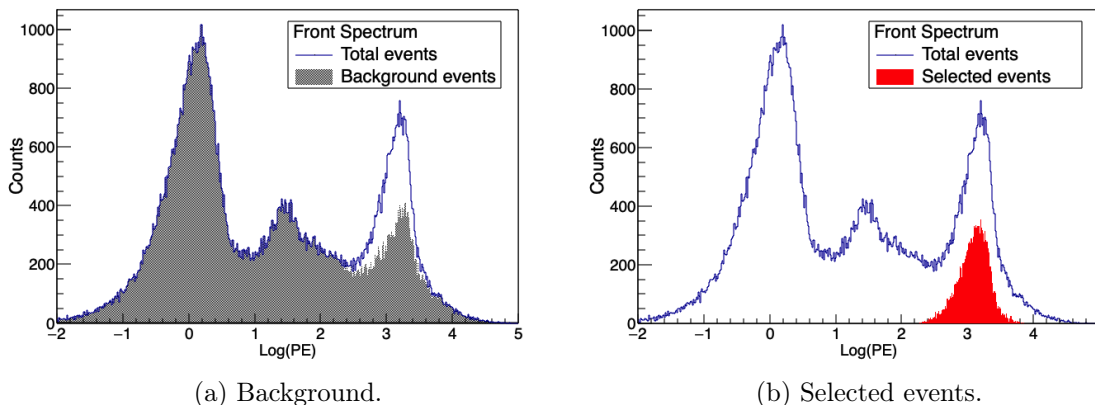


Figure 8: Background and selected events obtained through cuts applied on the number of PEs collected by each ARAPUCA, got comparing front and back spectra.

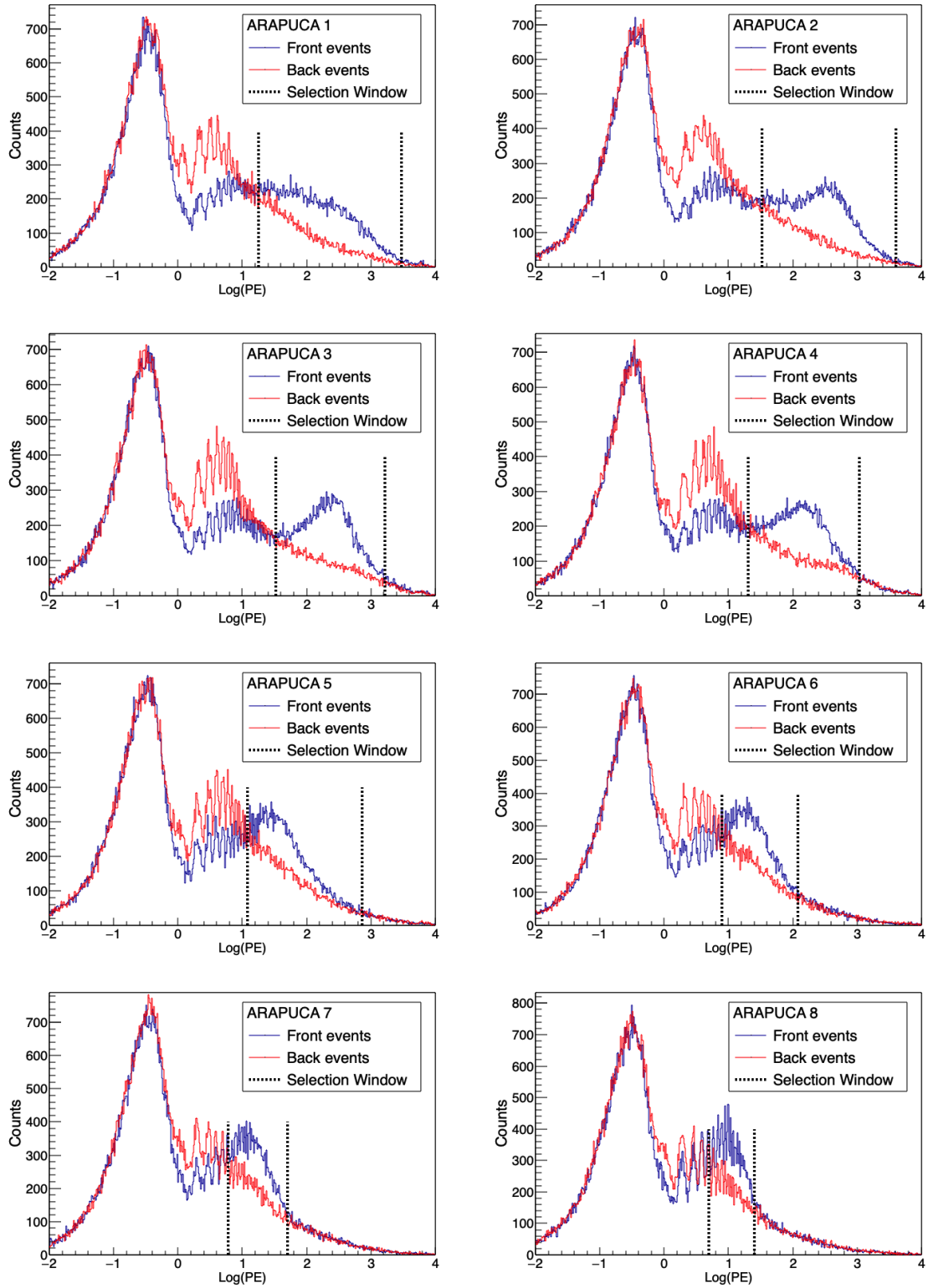


Figure 9: Front (blue) and back (red) Log(PE) spectra for the eight ARAPUCAs, and the cut applied (black). The cut consists in removing events for which the back spectrum (red) has more events respect to the front spectrum (blue).

3.3 ARAPUCAs multi-channel information

Each ARAPUCA is read out by an independent SSP channel, the segmented information can be used to study the track geometry. The number of PEs measured by each ARAPUCA must match the profile of the expected number of photons hitting the ARAPUCA array given a track geometry, with the track geometry provided by the hodoscope. The ratio between the number of PEs collected and the number of photons hitting each ARAPUCA depends only on their intrinsic features (geometrical dimensions, number of SiPM, wavelength shifter, dichroic filter). It should be constant and independent of the track geometry and the number of photons generated by a track in the LAr. Inconsistency of these ratio means we are observing a track not compatible with the geometry provided by the hodoscope. In that experiment the 8 cells of which the ARAPUCA array is composed, have the same features so we expect them to behave in the same way. The determination of the number of photons hitting each ARAPUCA is shown in the next section (3.4).

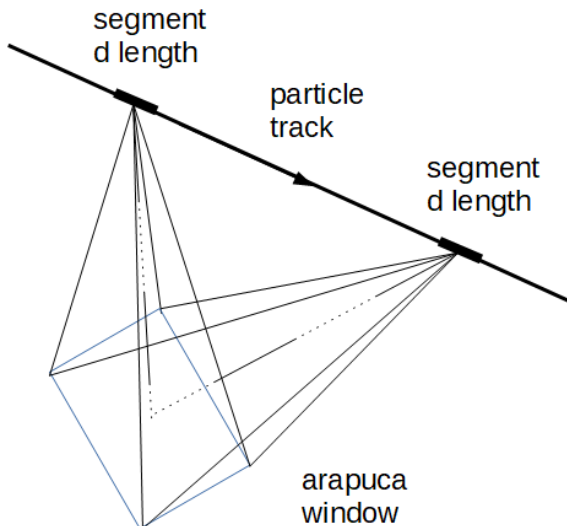


Figure 10: Track angular acceptance.

3.4 Light pattern

A charged particle crossing the volume of liquid argon will generate an amount of scintillation photons per unit of track length given by:

$$\frac{dN^\gamma}{dl} = \left\langle \frac{dE}{dx} \right\rangle \rho Y_\gamma q_p, \quad (1)$$

where $\left\langle \frac{dE}{dx} \right\rangle$ is the specific deposited energy ($MeV cm^2/g$), ρ is the density of the liquid in which the particle travels (g/cm^3), Y_γ is the number of photons emitted per unit deposited energy in the medium ($Y_\gamma = 5.1 \times 10^4 \gamma/MeV$), and $q_p = 0.78$ is the quenching factor [10, 11]. A crossing muon was assumed to be a MIP with a photon yield in liquid argon $Y_\gamma q_p = 4 \times 10^4 \text{ photons}/MeV$ and an energy deposit $\left\langle \frac{dE}{dx} \right\rangle \rho = 2.12 MeV/cm$.

The number of photons that arrive at the detector window due to a muon passing the argon volume is estimated as the product of the track integrated angular acceptance, A_Ω , and the number of emitted photons per unit length. This acceptance is defined numerically as:

$$A_\Omega = d \sum_{i=1}^N \Omega_i, \quad (2)$$

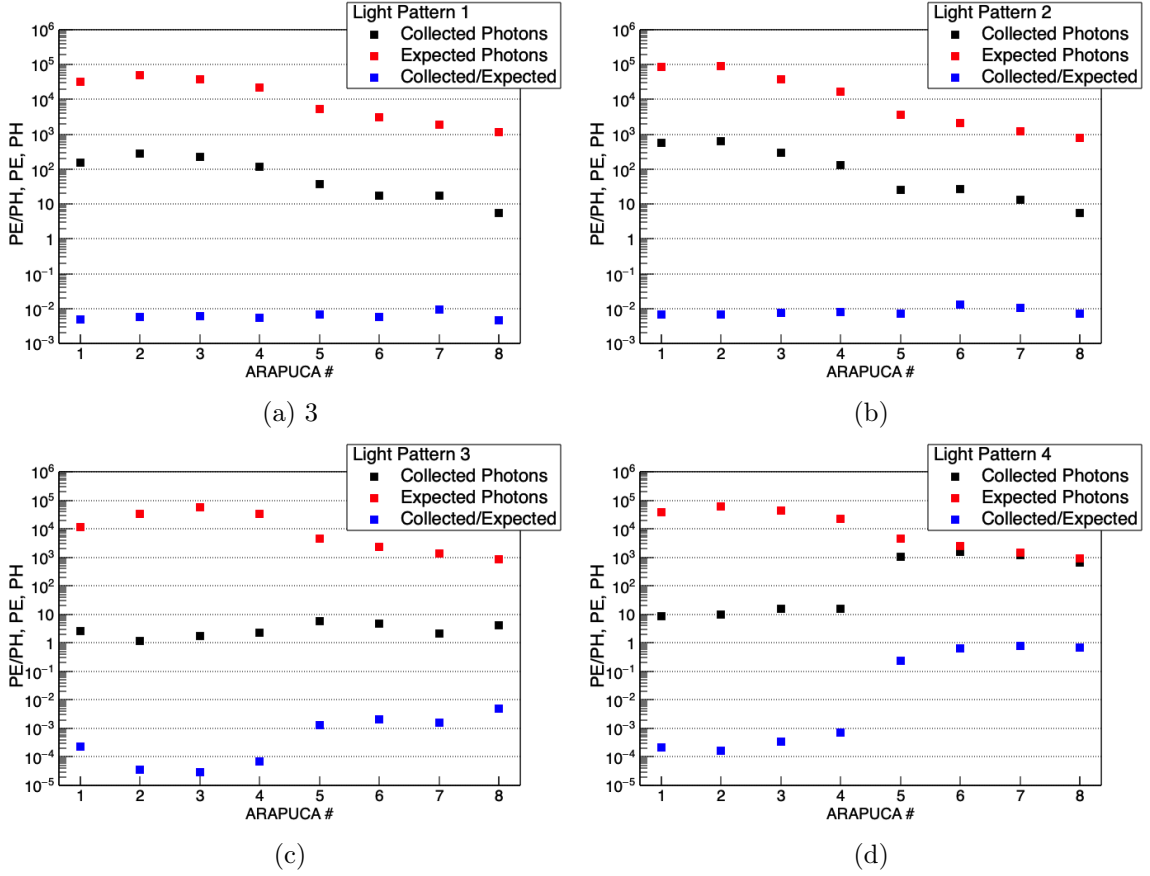


Figure 11: Comparison between the amount of light expected to arrive in each ARAPUCA (red), the number of PEs extracted from the waveforms (black) and the ratio between them (blue). Figures (a) and (b) show events following the pattern expected, Figures (c) and (d) show events not correlated with the trigger information. Blue points show the ratio of measured to expected number of photons. Statistical error bars are smaller than symbols.

where d is the length of a small (i.e. differential) segment of the muon trajectory and Ω_i is the solid angle of the pyramid with its apex at the center of that segment and its base given by the sensor window.

Ω_i is calculated using a set of formulas given in reference [12]. Figure 10 illustrates track segments and their correspondent Ω_i .

The total number of photons arriving (PH) at the ARAPUCA window is obtained as:

$$PH = \frac{1}{4\pi} A_{\Omega} \frac{dN^{\gamma}}{dl}. \quad (3)$$

The expected light calculated by the formulas and the number of PEs measured were compared, as displayed in Figure 11 for a few example tracks. There is a reduced set of events for which the expected and detected light follow the same shape pattern. It is expected that the absolute efficiency per ARAPUCA is a constant number smaller than 1. As mentioned previously, the efficiency is defined as the ratio between the number of PEs collected by the ARAPUCA and the number of photons arriving at the ARAPUCA window (PH) for a valid track event. Figure 11 demonstrates, for a valid track Figure 11a, the remarkable discrimination power of the ARAPUCA showing how the distribution of the collected light closely follows that expected for the illumination light, scaled down by a constant smaller than one that is directly related to the efficiency of the device. Also, for a different valid track such as in Figure 11b, that constant must remain the same within errors. Furthermore, Figure 11a and Figure 11b show that the ratios are similar for the 8 ARAPUCAs

used in the experiment. Figure 11c and Figure 11d also show that the same discrimination power allows filtering events where the shape of the distribution of the light collected by the ARAPUCAs do not follow that of the expected illumination. These tracks are due to MIPs that partially illuminated the ARAPUCAs and were mistakenly catalogued by the hodoscope with the wrong geometry due to hot PMTs and coincidental PMT events.

The criteria to separate valid from invalid tracks followed a χ^2 requirement as explained in section 3.6.1.

3.5 Correlation between collected and expected light.

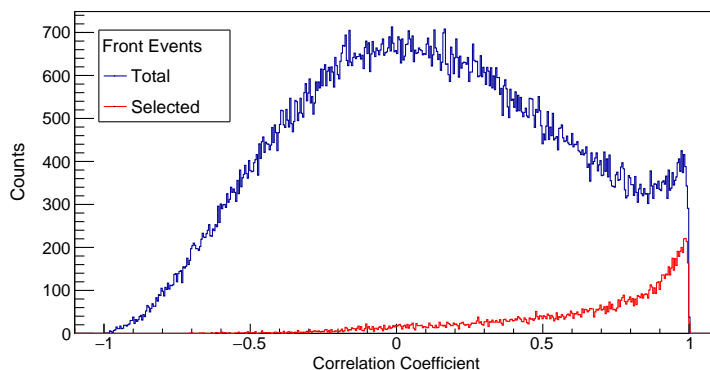


Figure 12: Correlation between PE_i and PH_i for the eight ARAPUCAs. Blue is for all the events, red for the events with the PE numbers, recorded by each ARAPUCA, in the range determined from the back and front spectra analysis.

After the selection based on front versus back spectrum discrimination, made in section 3.2, the events left are 14,811. The cut applied is crude and the data set is still contaminated with background. A second background rejection can be made utilizing the segmentation of the detector given by the 8 ARAPUCA cells shown in section 3.4.

Comparing the amount of expected light coming from the analytical formula and the number of PEs from waveforms, leads us to the determination of good tracks. In Figure 11 the number of PEs measured (black), the number of landing photons (PH, in red), and their ratio (blue) are displayed for each ARAPUCA, for a few tracks. There is a reduced set of events for which the expected and detected light follow the same pattern Figure 11a and Figure 11b. As an estimator for light pattern information we used the correlation between the measured PE number and the calculated number of photons landing on the ARAPUCA for each ARAPUCA in the event. The measure of correlation used is given by the Pearson correlation coefficient defined as

$$C = \frac{\sum (PE_i \cdot PH_i) - \sum PE_i \cdot \sum PH_i / 8}{\sqrt{\sum (PE_i^2) - (\sum PE_i)^2 / 8} \cdot \sqrt{\sum (PH_i^2) - (\sum PH_i)^2 / 8}} \quad (4)$$

where PE_i is the number of collected photo electrons in the i -th ARAPUCA and PH_i is the number of expected photons arriving on the i -th ARAPUCA surface. The i index goes from 1 to 8.

Figure 12 shows the correlation parameter for the total number of events (blue) and for the events passing the cut on the spectra (red). Most of the events passing the cut are peaked around $C = 1$ indicating a good correlation between the eight ARAPUCAs. However there are some events with $C \leq 0$. A second requirement on the correlation parameter is done, selecting events with $C \geq 0.7$. After that the total number of selected events is 13005. This number is the total for 366 hours of running time at a rate of 0.010 Hz.

The number of events selected is in a very good agreement with the rate expected from cosmic ray muon flux through the hodoscopes, obtained analytically, calculating the cosmic ray flux [14] through the hodoscope geometry getting $0.011 Hz$ and doing a simulation of the muons crossing the hodoscope: $0.0105 Hz$.

Figure 14a shows the common logarithm of the ratio between the sum of the photo electrons measured and the sum of the estimated number of arriving photons on each ARAPUCA, comparing all the data (blue spectra) and the selected dataset (red spectra) using the combination of both spectra selections and correlation requirement.

3.6 Efficiency analysis

The selected data set is then used to perform the efficiency analysis. The efficiency is defined as the ratio between the number of measured photons and the estimated number of arriving photons for each ARAPUCA:

$$\mathcal{R}_i = \frac{PE_i}{PH_i} \quad (5)$$

Figure 13 shows the ratio distribution for the eight channels. Furthermore, the ratio between the sum of the number of photoelectrons collected by all ARAPUCAs divided by the sum of the number of expected photons landing on all ARAPUCAs is considered.

$$\mathcal{R}_{TOT} = \frac{\sum_{i=1}^8 PE_i}{\sum_{i=1}^8 PH_i} \quad (6)$$

In Figure 14a is reported $Log(\mathcal{R}_{TOT})$ (for better visualization) for all the data (blue) and the data selected through spectra analysis and correlation cut (red), called "*Dataset 1A*". Three metrics for analysis were used, finding similar results reported in table 1:

- log-normal fit
- robust statistic
- bootstrap procedure on a reduced dataset

The first two methods were used on the data selected "*Dataset 1A*" and the last one applying a further restriction on the data, getting a reduced dataset (called "*Dataset 1B*"). Details about the performance of each metric can be found in the Appendix. Table 1 displays the ARAPUCA efficiency values measured by all metrics.

ARAPUCA	Mean (%)	Median (%) Fit result	Median (%) Robust stat.	MAD (%)
TOT	0.78 ± 0.02	0.80	0.77	0.41
1	0.74 ± 0.02	0.80	0.75	0.46
2	0.77 ± 0.02	0.85	0.80	0.55
3	0.80 ± 0.02	0.84	0.77	0.55
4	0.77 ± 0.02	0.71	0.66	0.42
5	0.75 ± 0.02	0.67	0.64	0.35
6	0.77 ± 0.02	0.69	0.65	0.36
7	0.77 ± 0.02	0.70	0.67	0.37
8	0.80 ± 0.02	0.80	0.75	0.40

Table 1: Ratio values from the three analysis. The error on the fit parameter associated to the median is negligible.

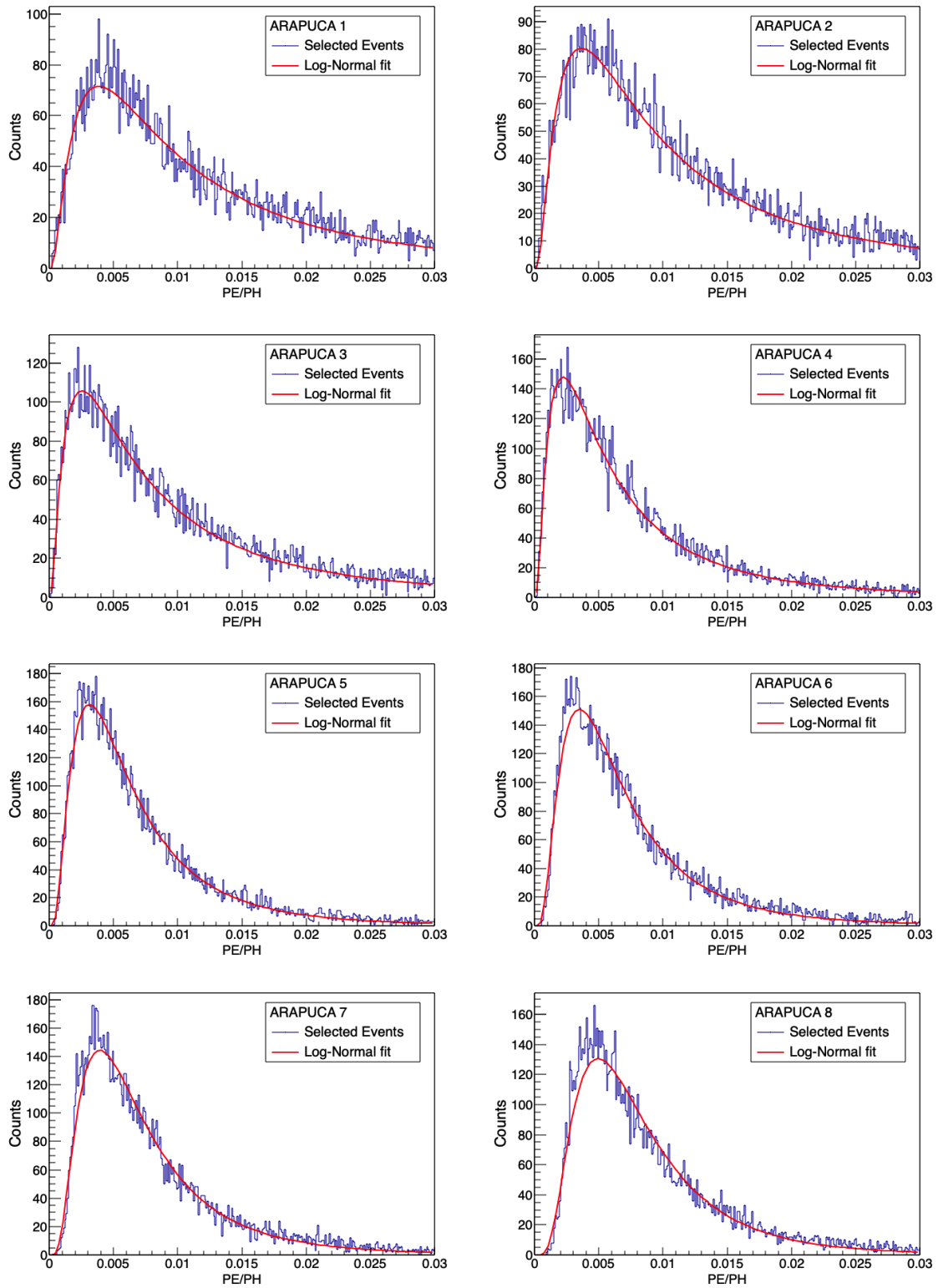


Figure 13: Ratio between the photo electrons measured and the estimated number of arriving photons per each ARAPUCA, of the data selected ("*Dataset 1A*").

3.6.1 χ^2 requirement on light patterns

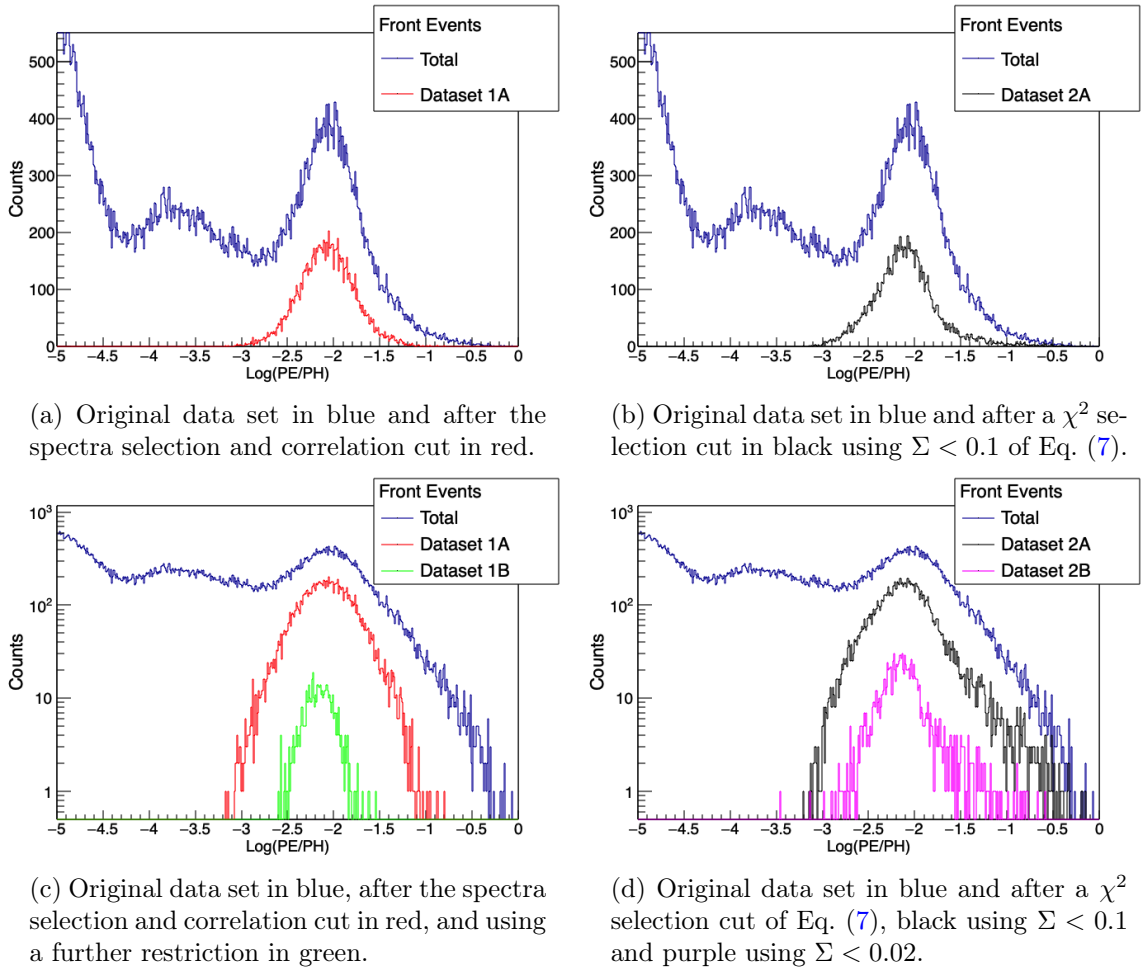


Figure 14: Comparison between the two kinds of cut applied to the original data set (blue spectra) of the ratio between the photo electrons collected sum and the estimated number of arriving photons sum. In Figure (a) and (c) are reported the selected datasets using the cut based on the spectra analysis and correlation condition, in figure (b) and (d) are reported the selected datasets using the χ^2 approach, described in section 3.6 Eq. (7).

A second criteria of data selection based on a χ^2 requirement on the ratio \mathcal{R}_i , was applied to the original dataset before any cuts (all the events), in order to check the goodness of the spectra selection and correlation requirements.

$$\Sigma = \frac{1}{8} \sum_{i=1}^8 \left(\frac{\mathcal{R}_i - \mathcal{R}_{TOT}}{\mathcal{R}_i + \mathcal{R}_{TOT}} \right)^2 \quad (7)$$

Requiring a condition on Σ we can select a certain amount of events. A smaller Σ means a better match between collected and expected photons. The conditions on Σ were determined in order to get the same amount of data of the other cuts, and the same three analysis were performed: robust statistic and log normal fit for a dataset using $\Sigma < 0.1$ ("Dataset 2A") and bootstrap procedure for a reduced dataset using $\Sigma < 0.02$ ("Dataset 2B").

3.6.2 Results

The data sets got through the two selection methods were tested increasing the requirements on the cuts, in the first case using the condition shown in Appendix A.3, in the second case

ARAPUCA	Hi-Low <i>Dataset 1B</i>	Low-Low <i>Dataset 1B</i>	Hi-Low <i>Dataset 2B</i>	Low-Low <i>Dataset 2B</i>
TOT	0.78 ± 0.02	0.78 ± 0.02	0.75 ± 0.01	0.75 ± 0.03
1	0.74 ± 0.02	-	0.72 ± 0.01	-
2	0.77 ± 0.02	-	0.75 ± 0.01	-
3	0.80 ± 0.02	-	0.77 ± 0.01	-
4	0.77 ± 0.02	-	0.74 ± 0.01	-
5	0.75 ± 0.02	0.81 ± 0.02	0.73 ± 0.01	0.75 ± 0.04
6	0.77 ± 0.02	0.75 ± 0.02	0.75 ± 0.01	0.78 ± 0.04
7	0.77 ± 0.02	0.72 ± 0.02	0.76 ± 0.01	0.78 ± 0.04
8	0.80 ± 0.02	0.79 ± 0.02	0.80 ± 0.01	0.79 ± 0.04

Table 2: Mean values of the ratio \mathcal{R}_{TOT} (Eq. 6) and \mathcal{R}_i (Eq. 5) for all the cells. Values for the two hodoscope configurations (Hi-Low and Low-Low) are reported, using the two selection criteria: spectra analysis and cut on the χ^2 (Eq. 7).

using $\Sigma < 0.02$ from Eq. (7). These procedures reduced to $\sim 10\%$ both the selected data sets (shown in Figure 14). In both cases the mean values of each ARAPUCA ratio became compatible with the median values found.

A similar analysis was made for the Low-Low hodoscope configuration using 3 MeV/cm of energy loss, reflecting the fact that the average muon energy increases for more horizontal events [13]. Due to the geometry of the tracks only the lower four ARAPUCAs are taken into account in the Low-Low configuration. The upper four have a small acceptance and the ratio \mathcal{R}_i (Eq. 5) is affected by large fluctuations because the number of photons detected is dominated by Poisson statistics. Table 2 shows the results from the two selection criteria for the two configurations. The ARAPUCA efficiency given by the median of the individual cells is $\mathcal{R} = (0.77 \pm 0.02)\%$. The TallBo7 test did not provide a measurement of after pulse and cross talk. The efficiency values reported here do not take into account their contribution. However, an estimation of $(31 \pm 7)\%$ of after pulse and cross talk is obtained from ProtoDUNE [15] preliminary analysis, where the same kind of SiPM were used and run in similar bias conditions. Adjusting by 31% the detection efficiency of the ARAPUCA detectors becomes $\epsilon = (0.60 \pm 0.02)\%$.

4 Conclusions

The Fall 2017 TallBo experiment has been successful in testing ARAPUCA photon detectors. Two of the features of the current ARAPUCA photon detector design were used to be able to filter the data offline. The single face detection and the fine segmentation of the ARAPUCAs allowed the offline analysis to separate events from background. The segmentation of the ARAPUCA detector validated the geometry given by the hodoscope. In the end an accurate absolute efficiency of 0.6% was determined by three different methods. That absolute efficiency is higher than efficiency measurements reported by previous experiments at TallBo using scintillation bars and wavelength shifters.

It is also worth mentioning that the ARAPUCAs only used 4 SiPMs per board, the filter to sensor aspect ratio was 35 which shows a remarkable improvement in the equivalent photon collection area given by the light-trap effect in the ARAPUCA.

Future work will study improvements in the internal reflective surfaces of the ARAPUCA, wavelength shifter thickness and adherence which should help increasing the light collection. A step forward in the development of ARAPUCA is the active ganging of SiPMs to lower

the number of readout channels per module and the use of the two faces of the detector for photon detection, having filters on both sides.

A Analysis metrics

A.1 Log-normal fit

A first analysis is made by fitting the ratio distribution with a Log-Normal distribution:

$$f(x) = \frac{1}{x\sigma\sqrt{2\pi}} e^{-\frac{(\ln(x)-\mu)^2}{2\sigma^2}} \quad (8)$$

This choice is driven by the $\text{Log}(\mathcal{R}_{TOT})$ which seems to follow a Gaussian distribution. The values of the Mean, Median, Mode, Variance and Standard Deviation are obtained by the relations satisfied by the parameters of the Log-Normal distribution:

- Mean: $e^{\left(\mu + \frac{\sigma^2}{2}\right)}$
- Median: e^μ
- Mode: $e^{(\mu - \sigma^2)}$
- Variance: $(e^{\sigma^2} - 1) e^{(2\mu + \sigma^2)}$
- Standard Deviation: $\sqrt{(e^{\sigma^2} - 1)} e^{\left(\mu + \frac{\sigma^2}{2}\right)}$

The error propagation, from the error in the fit, gives for the median the value:

$$\Delta_{Median} = e^\mu \cdot \Delta_{\mu} \quad (9)$$

A.2 Robust statistic

Because of the presence of outlier events, such as the ones in the far tail of the spectrum, a robust statistic data analysis is made for the data relative to the single ARAPUCA (\mathcal{R}_i) and their sum (\mathcal{R}_{TOT}), using median and the median absolute deviation (MAD) to build a robust score defined as:

$$\mathcal{S}_i = \frac{(\mathcal{R}_i - \text{median}_{j=1,\dots,n}(\mathcal{R}_j))}{MAD} \quad (10)$$

Then the median of the data set composed by the data which passes the requirement $\mathcal{S}_i < 2.5$ is calculated.

A.3 Strong correlation

Finally a restricted data set, obtained with a further strong condition on the light pattern, is analyzed.

The strong condition consists in requiring that all ARAPUCAs have the ratio \mathcal{R}_i similar to each other:

$$\frac{1}{2} \cdot \mathcal{R}_j \leq \mathcal{R}_i \leq 2 \cdot \mathcal{R}_j \quad (11)$$

This condition reduces the data set to be $\sim 10\%$ of the one used in the previous two analysis.

A bootstrap procedure is used to find the average values of the ratio and their errors, generating 10 thousand data sets, each of them composed by random extraction of events, from the original data set.

B Acknowledgements

The authors would like to thank A. Hahn, R. P. Davis, W. Miner, K. Harding for their technical support at PAB. We also thank the whole Indiana University team with whom this experiment was performed. We also thank Eileen Hahn for her invaluable knowledge and support for the wavelength shifter coatings of filters and reflectors, and also Kenneth Treptow for his technical support in assembling the ARAPUCA's module. This work has been partially supported by the Brazilian agency FAPESP under grant no 2017/13942-5. Fermilab is Operated by Fermi Research Alliance, LLC under Contract No. De-AC02-07CH11359 with the United States Department of Energy.

References

- [1] B. Baller et al., *Liquid argon time projection chamber research and development in the united states*, Journal of Instrumentation, 9(05):T05005–T05005, may 2014.
- [2] DUNE Collaboration, B. Abi et al., *The DUNE Far Detector Interim Design Report Volume 1: Physics, Technology and Strategies*, arXiv e-prints, July 2018.
- [3] A. A. Machado and E. Segreto. *ARAPUCA a new device for liquid argon scintillation light detection*, JINST, 11(02):C02004, 2016.
- [4] B. Howard, S. Mufson, D. Whittington, B. Adams, B. Baugh, J.R. Jordan, J. Karty, C.T. Macias, and Pla-Dalmau. *A novel use of light guides and wavelength shifting plates for the detection of scintillation photons in large liquid argon detectors*, Nuclear Instruments and Methods in Physics Research, 907:9–21, 2018.
- [5] G. Cancelo, F. Cavanna, C. O. Escobar, E. Kemp, A. A. Machado, A. Para, E. Segreto, D. Totani, and D. Warner. *Increasing the efficiency of photon collection in LArTPCs: the ARAPUCA light trap*, JINST, 13(03):C03040, 2018.
- [6] S. Coutu et al. *Searching for TeV cosmic electrons with the CREST experiment*, Nucl. Phys. Proc. Suppl., 215:250–254, 2011.
- [7] D. Whittington, S. Mufson, and B. Howard. *Scintillation Light from Cosmic-Ray Muons in Liquid Argon*, JINST, 11(05):P05016, 2016.
- [8] G. Drake P. DeLurgio, Z. Djuric and M. Oberling. *SSP User Manual*, Technical report, Argonne National Laboratory, 9700 S. Cass Avenue, Lemont, IL 60439 USA, 2016.
- [9] L. Condat. *A direct algorithm for 1-D total variation denoising*, IEEE Signal Proc. Letters, 20(11):1054–1057, 2013.
- [10] T. Doke, H. J. Crawford, A. Hitachi, J. Kikuchi, P. J. Lindstrom, K. Masuda, E. Shibamura, and T. Takahashi. *Let Dependence of Scintillation Yields in Liquid Argon*, Nucl. Instrum. Meth., A269:291–296, 1988.
- [11] T. Doke, A. Hitachi, J. Kikuchi, K. Masuda, H. Okada, and E. Shibamura. *Absolute Scintillation Yields in Liquid Argon and Xenon for Various Particles*, Japanese Journal of Applied Physics, 41:1538, March 2002.
- [12] R. J. Mathar. *Solid angle of a rectangular plate*, Technical report, Max-Planck Institute of Astronomy, Königstuhl, 17, 69117 Heidelberg, Germany, 2015.
- [13] M. Tanabashi et al. (Particle Data Group). *The review of particle physics*, Phys. Rev. D, 98:030001, 2018.

- [14] Prashant Shukla. *Energy and angular distributions of atmospheric muons at the earth*, Nuclear Physics Division, Bhabha Atomic Research Centre, Mumbai 400085, India. Homi Bhabha National Institute, Anushakti Nagar, Mumbai 400094, India, 2018.
- [15] DUNE collaboration. First results on protodune-sp lartpc performance from a test beam run at the cern neutrino platform. FERMILAB-PUB-20-059-AD-ESH-LBNF-ND-SCD, 2020.